Modelling the Thermal Conductivity of Thermal Barrier Coatings

J.-M. Dorvaux, O. Lavigne, R. Mévrel, M. Poulain, Y. Renollet, C. Rio
ONERA - Materials Science Department
29, av. de la Division Leclerc
92322 Châtillon Cédex
France

ABSTRACT
The thermal conductivity of ceramic coatings is a function of the thermal conductivity of the individual constituents (nature of phases, presence of point and planar defects, etc.) and of the morphology of the coating (pores, cracks). This latter aspect is particularly important for TBCs as it explains why their thermal conductivity is significantly lower than the corresponding values for dense materials.
This paper presents a model developed to calculate the thermal conductivity of porous and microcraked ceramic coatings based on a finite difference method applied on digitised images of yttria partially stabilised zirconia (YPSZ) coatings deposited by plasma spraying. The influence of the different types of morphological features on the thermal conductivity is discussed.

1. INTRODUCTION

Thermal barrier coatings are constituted of a ceramic external layer, most generally composed of partially stabilised zirconia (ZrO_2-6 to 8wt% Y_2O_3) deposited on top of an oxidation resistant metallic layer (MCrAlY alloy or modified aluminide). Their main function is to thermally isolate the superalloy components, blades or vanes, which they protect from the hot gases circulating in the turbine. Typically, the use of a 250 µm thick ceramic layer can provide about 200°C temperature reduction on the metallic part, thus prolonging its lifetime, reducing thermal transients, etc. [1].

Up to now, most of the efforts dedicated to thermal barrier coatings have been focused on the obtention of performant reliable systems and a predominantly empirical approach has permitted their introduction in service even on highly stressed components such as first stage blades [2].

Only recently, as witnessed for instance by the dedication of a full session during a recent TBC workshop [3] and on-going research programmes [4], significant attention has been increasingly directed towards characterising, understanding and lowering thermal conductivity, an altogether essential property for these systems.

Zirconia-based thermal barrier coatings exhibit already low thermal conductivities (typically between 1 and 2 W/m.K). These low values of thermal conductivity arise both from the intrinsic value of dense partially (and fully) stabilised zirconia materials and from the heterogeneous microstructure of the coatings deposited by plasma spraying or EBPVD (electron beam physical vapour deposition).

The introduction of a stabiliser, required to avoid the detrimental effect of monoclinic to tetragonal phase transformation at typical service temperature, is accompanied by the incorporation of a substantial amount of vacancies. Thus, in the case of yttria stabilised zirconia, the substitution of two tetravalent zirconium ions by trivalent yttrium ions is accompanied by the incorporation of one oxygen vacancy. For PSZ containing 8wt% Y_2O_3, this corresponds to a vacancy content of the order of 4.4 mol.%, providing an efficient source of scattering for phonon propagation. This also explains why the thermal conductivity of these materials is a decreasing function of the yttrium content (at least for relatively low stabiliser contents [5, 6]). Another way of decreasing the intrinsic thermal conductivity of ceramic layers would be to substitute zirconium ions with heavier metallic ions [7, 8], an approach followed by Maloney et al. [9] with a work on CeO_2-Y_2O_3 system, at the expense though of an increase in density.

Another efficient way to decrease the thermal conductivity of a material is to introduce microstructural defects such as pores, voids, microcracks which constitute obstacles against the through-thickness heat transfer propagation. Fortunately, the presence of such defects, produced during fabrication, seems to be indispensable for the thermomechanical resistance of these systems. It is doubtful however that their distribution in existing coatings is optimised regarding the thermal properties and, in order to design more performant TBCs, it now appears necessary to be able to characterise and understand the relationship between thermal conductivity and microstructural features constituting these heterogeneous materials.

It must be reckoned that guidelines that can be derived from the literature, in particular from models relating morphology (porosity) and thermal conductivity of solid materials are of limited usage in the case of thermal barrier coatings due to the complexity of the microstructures.

A variety of models have been developed to estimate the thermal conductivity of multiphased solids, in particular porous materials. Most of them assume the material constituted of a dispersion of a more or less concentrated and randomly distributed second phases. While early models proposed by Maxwell [10], Eucken [11], Russel [12] and Bruggeman [13] for example, consider only spherical particles, improved versions elaborated by Murabayashi [14], Schulz [15], Koh and Fortini [16], Cunningham [17] and McLachlan [18] consider ellipsoids characterised by shape and orientation factors.

As a general rule, the thermal conductivity λ of a porous solid derived with these models can be expressed as :

$$\lambda/\lambda_0 = f(\varepsilon, n_i)$$

where λ_0 is the thermal conductivity of the pore-free solid, ε is the volume fraction of the pores and n_i are adjustable parameters, to be determined empirically, related to the shape and/or orientation of pores .

To evaluate the validity of these models, several authors have examined the analytical results given by some of these models in light of experimental values on different systems [19, 20, 21, for example]. Examining experimental data on alumina, graphite, uranium dioxide, sandstone, silica brick and limestone, and with

Paper presented at an AGARD SMP Meeting on "Thermal Barrier Coatings", held in Aalborg, Denmark, 15-16 October 1997, and published in R-823.

porosity up to 75%, Rhee [19] found a satisfactory correlation with the equation proposed by Aizanov and Domashnev [22]. For El-Fekey et al. [20] who evaluated the Maxwell, Loeb and Murabayashi models on thoria compacts with porosities up to 46%, the Murabayashi model [14] yields the best result among the three. More recently, Jackson et al. [21] found that McLachlan's equation [18] comes closest to modelling the experimentally measured thermal conductivity of AlN-Ln_2O_3 systems.

Remarking that the experiments considered may not be suited to determine the quality of theoretical calculations, due to various experimental inaccuracies and simplifications, Bakker et al [23] have computed the influence of pores of different shapes (cylinders, spheres, ellipsoids) with the FEM technique. The comparison with the equations describing the effect of inclusions on the overall thermal conductivity shows that the analytical equation of Schulz [15] gives a good description of such materials.

A full review of all the models is beyond the scope of this article. However, the puzzling diversity of conclusions derived by these authors point out to the fact that all these models with simple algebraic expressions assume that the porosity can be experimentally assessed with a very limited number of parameters (the pore volume fraction ε and adjustable parameters), which singularly restricts their predictive capacity.

To overcome these shortcomings, several authors have developed more sophisticated theoretical approaches as well as finite element calculations to estimate the effective thermal conductivity of multiphase materials.

Tzou [24] estimated the thermal conductivity starting from a general field theory (supposing uniformly distributed internal cavities), deriving tractable analytical expressions for simple pore geometries, i.e. insulated spherical cavities and penny-shaped cracks.

In a more sophisticated approach, Furmanski [25] developed an effective macroscopic description for heat conduction in heterogeneous materials using an averaging technique and Green's function method and applied it to describe a model composite with randomly oriented parallelepiped inclusions distributed in an epoxy matrix.

The expressions obtained with these approaches become readily complex and apparently they have been used up to now only in the case of uniform distributions involving rather simple geometrical shapes for the pores (ellipsoid, cubes). For materials having complex pore microstructures, such as those met in plasma sprayed coatings, and in order to be closer to the real structure (interconnected porous structure), however, numerical schemes appear to be the most promising approaches.

With the objective of extending the rather simple analytical approaches (and poorly predictive) proposed by McPherson [26] and by Moreau et al. [27] on the thermal conductivity of plasma sprayed coatings (and later improved by Bjorneklett et al.[28]), Hollis [29] developed a numerical scheme in which the actual pore structures of vacuum (VPS) and air (APS) plasma sprayed tungsten coatings are used as the basis of finite-element models to calculate the effect of pores on the thermal conductivity of plasma sprayed coatings. If, for VPS coatings, whose pore distribution and shapes are relatively simple, this approach gives a reasonable agreement between calculated and experimental values (respectively 70% and 60% of the bulk value), for APS coatings, instead, a large discrepancy exists between calculated and measured values. This is attributed to the complex pore structure, which cannot be properly taken into account by the limited areas on the cross sectional micrographs serving as input information into the calculation.

In a study on the thermal conductivity of UO_2 pellets, Bakker [30] used a finite element method to compute the conductivity of a matrix containing a dispersed phase (pores). Starting from a photograph of a cross section, the microstructure of the material is described as a triangular mesh used as input data. Arbitrary temperatures are imposed on the upper and lower boundaries of the corresponding area (other boundaries are taken adiabatic) and the FEM program computes the conductivity from the thermal flux profile. As explained later, it remains doubtful whether this type approach can be extended to large areas, keeping memory storage reasonable.

In the work presented here, the objective was to develop and evaluate an alternative approach, based on a finite-difference calculation for computing the thermal conductivity of thermal barrier coating, using as input data digitised images of the real material. With this method, the morphology of the ceramic coating, as complex as it can be, is properly taken into account.

2. CHARACTERISATION OF TBCs POROUS STRUCTURE

In order to provide data to the thermal conductivity calculation software, reliable procedures have been developed to quantify the real TBCs porous structure. The success of the modelling strongly depends on the accuracy and reliability of the results of these procedures. The complete microscopic characterisation of the TBC morphology involves numerous steps as sample preparation, image acquisition, image analysis and validation with macroscopic porosity determination.

Sample preparation

A correct and reproducible metallographic preparation of plasma sprayed ZrO_2 coatings is not straightforward but is essential for obtaining a representation of the real porous structure. Porosity determination by quantitative image analysis and numerical calculation of the thermal conductivity will give reliable results provided that no error is introduced at the sample preparation stage.

Materials

All investigations are performed on a 1 mm thick free standing TBC plasma sprayed by SNECMA, initially on a HastelloyX substrate without any bondcoat. The powder is a commercial 8 weight% yttria partially stabilised zirconia spray dried powder (HCST Amperit 827.423).

Sample preparation

The following procedure has been set up. The free standing coating is vacuum impregnated (Struers/Epovac, P~100 mbar) with a superfluid epoxy dye (Struers/Epofix 301) before sectioning. Sample slices are then cut off with a precision saw (Struers/Accutom-2) using a thin diamond wheel and the lowest rotation and sample forward speeds to avoid any damage. The slices are then manually polished according to the following steps : 1200 then 4000 SiC papers for grinding, polishing using a 3 µm diamond spray first on a hard cloth (Struers/Pan W, blue lubricant) then on a smoother cloth (Struers/DP-Mol, pink lubricant), final polishing with a ¼ µm diamond paste. Polishing quality and absence of pull-outs are checked with light microscopy after each step. For scanning electron microscopy observations a ~20 nm thick conducting carbon layer is vacuum sputtered within a Balzers MED010 unit.

Image acquisition

Cross sections of TBC prepared as previously described have been observed in a digital scanning electron microscope (Zeiss/DSM960). Backscattered electron mode is chosen preferentially to secondary electron mode due to the higher contrast between zirconia matrix and porosity (pores and cracks). The adopted acquisition conditions are the following : 15 kV acceleration voltage, 9 mm working distance, « low » electron current. Brightness and contrast are adjusted in order to obtain a reproducible grey level histogram (Fig. 1). Two magnification levels (180x180 μm^2 ; 45x45 μm^2) and two image resolutions (512x512 or 1024x1024 pixels) have been used for characterising the TBCs morphology. Their influence will be discussed later on (see § 4).

Signal to noise ratio is increased by pixel averaging so that a 1024x1024 pixels image acquisition takes about 400 seconds. Image acquisition is fully automated owing to computer assisted stage displacement. This allows a statistical characterisation of the samples.

Image analysis

Image analysis procedures have been developed with two objectives :

- provide binary images of TBC cross sections which will be used directly as input data for the thermal conductivity calculation software,
- quantify the porous structure in such a way as to be able to determine the contribution of each morphological feature to the thermal conductivity of a thermal barrier coating.

This will be the starting point for modelling thermal conductivity as a function of the morphology.

Thresholding

The transformation of SEM grey level images into binary images is the key step on which depends the reliability of the subsequent results. The threshold level is manually fixed on images with optimised and reproducible grey level histogram (Fig. 1).

This last one contains two peaks : a very sharp and intensive peak at the 0 level (black level) corresponding to the majority of the globular pores and a wider one centred at middle grey levels which includes cracks and zirconia matrix.

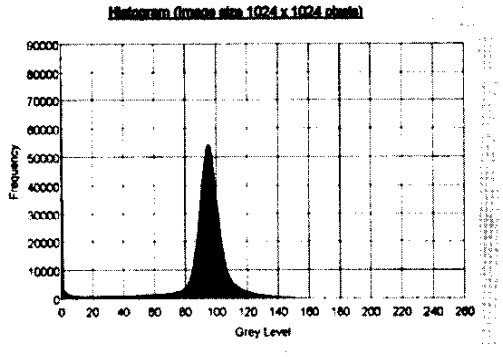

Figure 1: Grey level histogram.

The adopted threshold level which accounts for the whole porosity (pores and cracks) corresponds to the beginning of the lightening of isolated pixels in the solid phase (Fig. 2). This ensures its reproducibility.

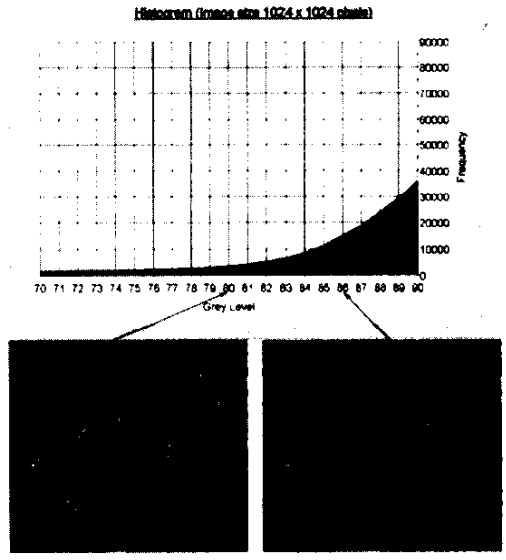

Figure 2: Thresholding.

Porosity separation

This procedure is based on opening and reconstruction image analysis operations. It creates three new images from the initial thresholded image : one containing the dispersed globular pores, one with the crack network and one with the globular pores and the cracks directly connected to them.

This fully automated procedure will be widely used to determine the contribution of each morphological feature to the conductivity (see § 4). A still more precise description can be achieved using the following procedure.

Porosity reconstruction

From an initial parent binary image it is possible to derive a series of images (about 300 or more according to the morphology complexity) with evolving porosity. This is done by applying a sequence of erosion image analysis operations to the parent image which leads to a final image containing only « ultimate erodeds ». These pixels exactly correspond to the globular pore centroïds. Starting from this new image, a step by step reconstruction of the porous features creates the derived images. The operation is ended when the initial total porosity is completely reconstructed (Fig. 5).

An application of this procedure in relation with the thermal conductivity computation will be shown in the last section.

Image assembling

This algorithm is developed to provide large size images of the samples which are more representative for the conductivity calculation. This is done by an automatic search of maximal overlap between two binary images from contiguous and slightly overlapping fields.

Analysis of globular pores

Each individual globular pore is characterised by a set of parameters (area, perimeter, Feret's diameters, number of neighbours,...). In this way different pore distributions (in number, surface,...) can be obtained (Fig. 3).

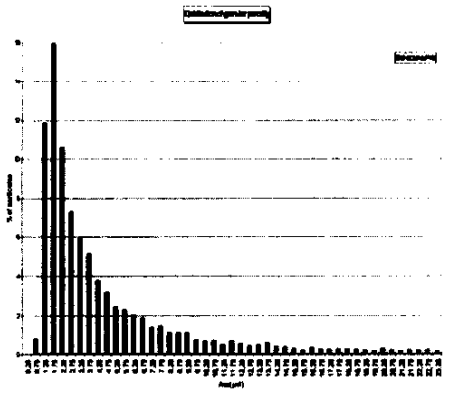

Figure 3: Globular pore distribution (% of particles versus area)

Analysis of the crack network

This procedure is based on the « skeletonization » (image analysis terminology) of the crack network, followed by a decomposition in juxtaposed segments of minimal fixed length. A distribution of these segments with regards to their orientation is then available (Fig. 4).

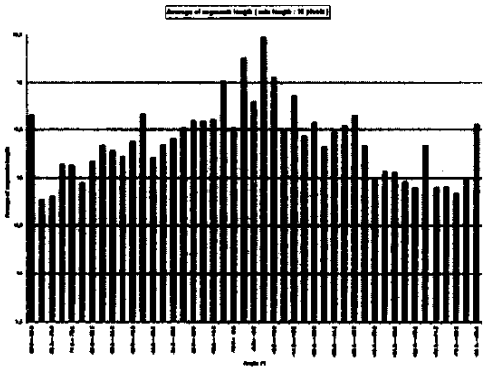

Figure 4: Segment orientation (average of segment length versus angle)

Porosity determination

The total porosity of a TBC can be estimated from binary images of cross sections using image analysis provided that the number of analysed fields is statistically relevant. A total of 105 images (180x180 μm^2 ; 1024x1024 pixels) corresponding to two transverse perpendicular cross sections have been considered. The mean porosity value obtained for this image set is 15% with a 2% standard deviation.

Furthermore the volumetric total porosity of the whole free standing coating (60x45x1 mm^3) has been determined to 12±1 % from water immersion experiments and X-ray diffraction theoretical density data. Closed porosity is less than 1 %.

The relatively good agreement between image analysis results and volumetric porosity shows that the sample preparation procedure as well as the thresholding one do not introduce too many artefacts. The higher value obtained by image analysis is attributed to some remaining pull-outs and mostly to the fact that backscattered electron detection slightly enlarges the narrowest cracks.

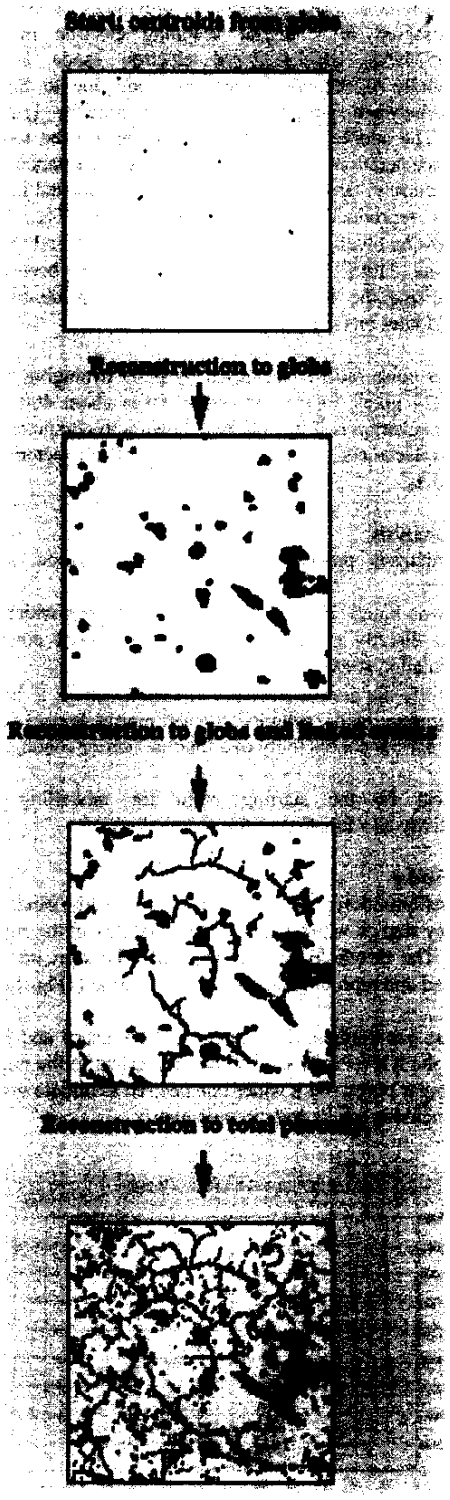

3. NUMERICAL COMPUTATION OF THE THERMAL CONDUCTIVITY

It has been shown that the morphology of a zirconia plasma sprayed coating is relatively complex in so far as it involves dispersion of pores with various sizes and shapes and connected crack network. As we are concerned with the influence of morphology on thermal conductivity and we want all the morphological information obtained with SEM to be taken into account, the modelling method must face this structure complexity without oversimplification.

Analytical or empirical models mentioned in the introduction only deal with simplified geometrical shape dispersions and are not well suited for connected porosity. The variety of pore structure families does not allow an efficient use of such models, which are generally restricted to one simple type of shapes and cannot handle connectivity effects with a fair accuracy.

Computations on very complex geometry are tractable with some numerical methods. The finite-element method is well known for its possibilities in this field. Recent works [29,30] demonstrate these capabilities by computing the thermal and electrical conductivities of porous metals or metallic oxides.

The finite-element method, among others, uses a grid representation of the geometry. The mesh properties of this grid are however submitted to some constraints. Then its application to very complex shapes may lead to some difficulties. As each shape to be modelled must be decomposed in simple geometric elements (triangles or quadrilaterals), the resulting amount of nodes and meshes may become tremendous when the geometry presents very small details. For example the minimal shape that we may encounter is a single square of one pixel size. If we want to decompose it in triangular or quadrilateral meshes, this single pixel produces, at least, four nodes. Continuity constraints on the neighbouring meshes may impose some grid refinements on the vicinity of this isolated pixel, even if the closest shapes are very large. As a consequence the resulting mesh density in the area close to this square may become very high. For thin cracks (their minimal thickness is one pixel) this may lead to more dense mesh distribution and untractable continuity constraints. Therefore, as the solution methods are generally global (e.g. they are often reduced to a minimisation problem), the associated algebraic system may reach an unpracticable size. So the finite element method seems to be difficult to apply in our field of study if no restriction on the geometry is acceptable.

On the other hand, the standard finite-difference method seems to undergo equivalent restrictions as it needs some grid representation, and therefore, some specific processing on the internal boundaries (e.g. boundaries between porosity and matrix).

However, this can be overcome if :

- the grid can be constructed directly from the input data image,
- the discretisation does not need specific processing on internal boundaries,
- the resulting set of algebraic equation remains practicable.

Specific implementation of the finite difference method

The grid construction may be reduced to a very simple process if we use a regular uniform mesh grid where nodes are simply defined by the pixels (square pixels) of the input image. With such a grid no geometric internal boundary information is associated with meshes. These information are related to the properties of each node (e.g. the local thermal conductivity) and are stored as coefficients of the partial derivative equation to be solved. The schematic representation of our problem is shown on figure 6 :

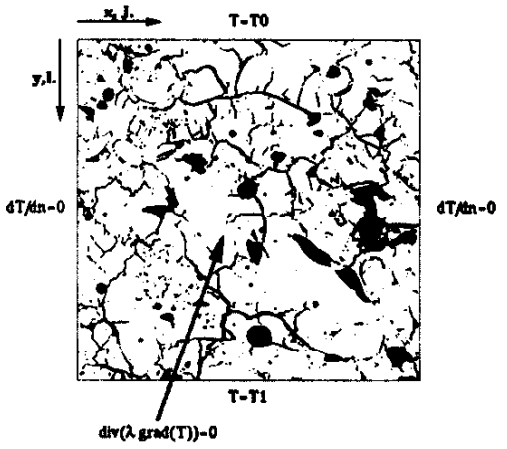

Figure 6: Problem definition.

Then we have to build the finite-difference equation to be solved for each node. This is done by means of the well known five points scheme, that is :

$$(A(i,j)+B(i,j)+C(i,j)+D(i,j))\mathbf{T}(i,j) = A(i,j)\mathbf{T}(i,j-1)+B(i,j)\mathbf{T}(i-1,j)+C(i,j)\mathbf{T}(i,j+1)+D(i,j)\mathbf{T}(i+1,j)$$

If we do not want to treat the discontinuities of these A,B,C,D coefficients with specific equations occurring when the local conductivity exhibits a step, an implicit way has to be found. For example the well known [31] five weighted conductivities scheme widely used in variable (but continuous) properties problems where the coefficients are defined by :

$$A(i,j)=1/2(\lambda(i,j-1)+\lambda(i,j))\,;$$
$$B(i,j)=1/2(\lambda(i-1,j)+\lambda(i,j))\,;$$
$$C(i,j)=1/2(\lambda(i,j+1)+\lambda(i,j))\,;$$
$$D(i,j)=1/2(\lambda(i+1,j)+(\lambda(i,j)))\,.$$

and which is of second order (for continuous properties) is not applicable in our case because it smoothes the discontinuities. Indeed, one can easily see that for small sized (e.g. one or two pixel thickness) objects this scheme leads to erroneous values as no node is assigned its real conductivity.

More suited schemes can be constructed using asymmetrical distributions of conductivity. For example the Upper Left scheme we commonly use is defined by :

$$A(i,j)=\lambda(i,j-1)\,;$$
$$B(i,j)=\lambda(i-1,j)\,;$$
$$C(i,j)=\lambda(i,j)\,;$$
$$D(i,j)=\lambda(i,j)\,.$$

Four first order distinct schemes can be constructed on this basis (the four corner implementations). It can be shown that they lead to a space transformation in the neighbourhood of discontinuities as they operate a small translation along bisectrix of i,j axes. For random geometries they are not strictly equivalent as they produce small variations (about 10^{-4} or less)

of the resulting computed conductivities, but as we will see below (Fig. 9) this is not the most critical source of uncertainties in the present problem.

For the main boundaries (e.g. the boundaries where Dirichlet or Neumann conditions are applied) we use the standard method, that is the image method based on the same scheme for Neumann condition (the Dirichlet condition does not need any computation as T is imposed).

When the temperature is known for each node, the average or equivalent thermal conductivity of the whole domain is computed from :

$$\lambda_m = \frac{e}{l}\frac{\int_0^l \lambda \frac{\partial T}{\partial y} dx}{T_1 - T_0}$$

where e is the height and l the width of the domain, the integration being done on one of the horizontal boundaries. The space step being constant, that integration can be performed with standard quadrature formulas.

The solver

The proposed scheme leads to a set of Nx-2*Ny linear equations to be solved. As we are concerned with large values of Nx and Ny (computation with Nx~4200 and Ny~5100 has been performed), the solver has to be as efficient as possible.

The first difficulty is to have the most compact form of the problem in order to reduce memory occupation. This can be done efficiently by reducing the coefficient storage.

With the definition of A,B,C,D we have seen before, it can easily be shown that, for a simple diphasic problem, we have to store only $2^3 + 2^2 + 2^3$ different configurations. So the storage for A,B,C,D can be drastically reduced provided that we can store some case index for each node.

As this case number is in the range of tens, an array of bytes is convenient. So the minimal storage required is :

- one Nx*Ny double precision array for **T**,
- one Nx*Ny byte array for case markers,
- 4*20 double precision scalars for coefficients,
- one Nx*Ny byte array for input data.

This is about 10 Moctets for a 1024x1024 problem and up to 210 Moctets for a 4200x5100 problem. So if the solver does not need intermediate storage, we expect that such problems can be solved on common 256Mo RAM computers. The solution method may be chosen with respect to this criterion. The two common approaches for this kind of solver are iterative matrix methods and iterative by points methods.

The first kind is well represented by the conjugate gradient method [32] which, as other matrix methods, does not satisfy our criterion. It needs, at least, two or three times the minimal storage defined above. So the maximal dimensions of the problems we could solve with such methods would be reduced by a factor of $\sqrt{2}$ or $\sqrt{3}$. Alternatively, we would need some supercomputer.Therefore, matrix methods are very efficient on computers with high vectorisation capabilities (as Cray for example), but seems to be less attractive on scalar or superscalar computers (such as common workstations) [33].
The second kind is commonly known as the Gauss or Gauss-Seidel method [32].

They can be implemented without extra storage so our criterion is satisfied. Provided that we are able to find some well suited (Fig. 7) convergence acceleration parameter (over-relaxed Gauss-Seidel method), they can outperform matrix methods when applied on scalar or superscalar computer [33], but they are notably less efficient when deep vectorisation is allowed.

So we have implemented an over-relaxed Gauss-Seidel solver which allows the solution of problems with sizes up to about 6000x6000 on our 512Mo RAM workstation. With the commonly used SEM magnification this theoretically allows the computation of TBC conductivity for thick samples (1.2x1.2 mm^2), or extended areas of relatively thin coatings (for example 0.20x36mm^2).

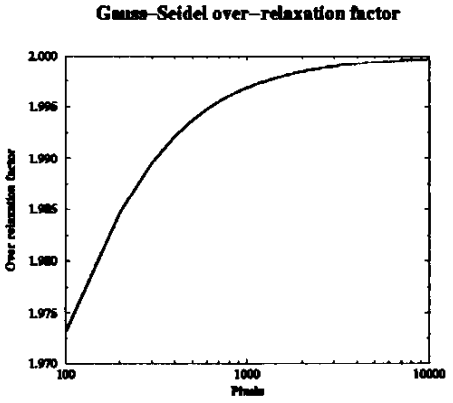

Figure 7: Convergence acceleration parameter.

For huge problems, the main limitation is the duration of computation. The following table shows computation duration in seconds for a standard 1024x1024 problem with 10^{-4} precision criterion (e.g. the convergence criterion on heat flux in relative form), for three different superscalar computers :

HP9000/780	DEC Alpha 500	Pentium Pro
260	405	1164

The computation was achieved with 3000 iterations using a convergence acceleration parameter of 1.997. The maximal residual error on heat flux (relative value) was about $9.4.10^{-5}$.

One can consider this case as the simplest one because the input data image was of medium complexity. For higher complexity input the maximal computation time may be twice the indicated time. For the 4200x5100 problem we have solved only on the HP workstation, the computation time was about 10 hours in the most difficult case. Notice that the complexity (which can be evaluated as some function of the number of porous objects) increases roughly as the area of the domain. Despite that, the relation between the size of the domain and the computation time which is a power function of the maximal dimension of the domain exhibits an exponent close to 3, which is the theoretical value for the over-relaxed Gauss-Seidel method.

The initial value for T may also strongly influence the speed of convergence. Our standard initialisation is the temperature distribution for the homogeneous medium. A possibly more efficient initial distribution may be constructed from the Richardson's extrapolation concept [34]. Let $\mathbf{T}_{1/2}$ be the solution of the problem for the domain reduced by a factor 2 in each dimension (e.g. we compute only one node out of two). This

solution may be achieved within a time $t_c/8$, where t_c is the computation time for the whole problem .

The values of T are then determined on alternate nodes using bilinear interpolation. The global cost of these two operations remains close to $t_c/8$. As we do not need an ''exact'' solution for $\mathbf{T}_{1/2}$, we can reduce the precision criterion in order to reduce this time. So the initial data construction has a cost less than $t_c/10$ for example. Our major expectation is that such an initialisation would be very close to the whole solution **T**. Then the amount of computation needed to obtain **T** would be substantially reduced.

Experiments have shown that the effective global computation time may be reduced by a factor of about 2 for low complexity input (globular porosity for example). For higher complexity input the time reduction is often imperceptible as small details (cracks for example), which are partially lost in the $\mathbf{T} \rightarrow \mathbf{T}_{1/2}$ input transformation, have a major contribution to the whole solution. So this is not a very efficient method for the reduction of computation duration because of its lack of generality.

Computation output

The computation program outputs some convergence information and the computed equivalent thermal conductivity. Therefore, the resulting array of temperatures is saved in a compacted binary file. This file can be read by another program for visualisation purpose. The temperature, its gradient, and the heat flux can be visualised by means of isovalue representation as shown on figure 8.

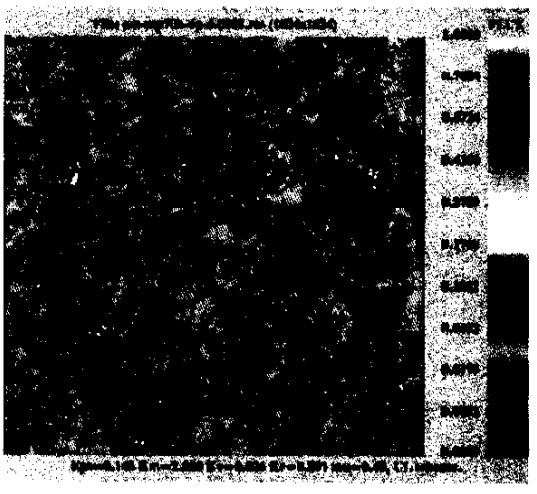

Figure 8: Heat flux representation.

Such representations performed on images with separated porosity give a qualitative useful description of the effect of each morphological feature on the heat transfer through a TBC.

4. APPLICATIONS

Before applying these tools to various TBCs, three major points have to be considered.

The resolution problem

The first one concerns the optimal choice for input image resolution. As figure 9 shows, the computed conductivity strongly depends on the input image dimensions.

Images of the same physical field with various resolutions (e.g. 256x256, 512x512, 1024x1024, 2048x2048 pixels) lead to four inputs which have been used for conductivity computation. An

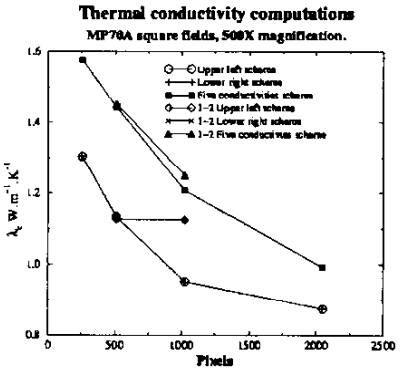

Figure 9: Thermal conductivity versus resolution.

extra 1024x1024 image (referenced 1-2) is obtained from the 512x512 one by a pixel duplication technique. The computed conductivity is a decreasing function of the resolution whereas the toral porosity is nearly a constant. As results for the 512x512 and the 1-2 cases are quasi identical we can assert this is not a discretisation effect. The main justification we found is the loss of small morphological details (loss of crack continuity for example) which results from the resolution decrease but does not strongly affect the total porosity. The computed conductivity seems to be related to the resolution by :

$$\lambda_c = \lambda_{\inf} + \frac{a}{N}$$

where λ_{inf} is the value we would obtain for an ideal resolution and N is the resolution expressed as the number of pixels on one side of the image. Thus we are able to find a resolution independent value of the thermal conductivity for each field if we have two different resolution input images. This is an easy thing to do as a 512x512 input image can be constructed from a 1024x1024 one by pixel destruction. So all the following results are presented with three values (the 1024 resolution, the 512 resolution computed values and the ideal resolution extrapolated value) for the computed conductivities.

The matrix thermal conductivity problem

The second problem concerns the conductivity data of the different phases. For the computations, the needed data are the morphology and the thermal conductivity of each phase.

For the porous one, we can use the thermal conductivity of air which is well known. The major problem is for the zirconia matrix thermal conductivity. At present only bibliographical values are available. They fall between 2 and 3 $W.m^{-1}.K^{-1}$ [5], so the related uncertainties on computed thermal conductivities are large. Some in-situ evaluations of the matrix conductivity are in progress by means of microscopic thermal diffusivity measurements on real TBCs. They may lead to more realistic values of matrix properties in a near future. In the meantime, we have used an arbitrary value of 2 $W.m^{-1}.K^{-1}$ for all computations.

The 2D to 3D effects

The third point is related to restriction on actual geometry. All the data and results we are able to obtain with these methods are

two-dimensional. Three-dimensional effects can heavily change the conductivity if inclusions have geometrical properties which cannot be evaluated with two-dimensional sections. As Bakker [29] mentionned, the three-dimensional problem is unreachable with current computers. Therefore the construction of the relevant three-dimensional input data sets would be unpracticable with the resolution we use. So the present work is limited to the two-dimensional approach. Fractographies performed on plasma sprayed TBCs suggest that the cracks, which are responsible of the main conductivity reduction, have depth/width ratios far exceeding one and a two-dimensional section is an acceptable representation for such geometries. But this is not the case for globular porosity.

Owing to these various uncertainties the computation results have to be considered indicative rather than exact.

Results

These tools were first applied to a free standing TBC plasma sprayed by SNECMA. Extensive analysis and computations were done on such coating in order to :

- test and validate the different procedures,
- study the influence of different classes of porosity on thermal conductivity.

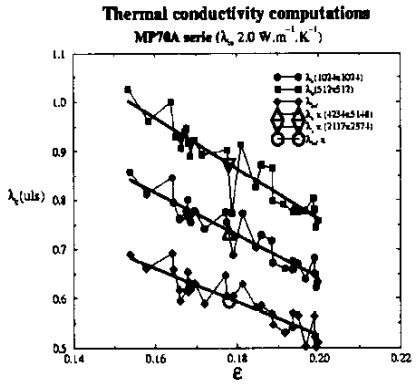

Figure 10: Plasma sprayed TBC computed thermal conductivity versus porosity.

A set of 35 adjacent (1024x1024 pixels) fields was obtained with the SEM. The thermal conductivity has been computed on each field and is represented versus porosity on figure 10

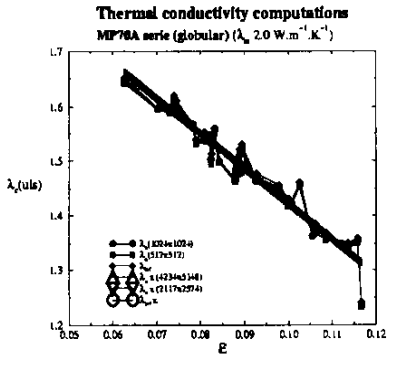

Figure 11: Globular porosity contribution.

(medium line). The lower line corresponds to ideal resolution images and is derived from calculations with 1024x1024 and 512x512 resolutions as explained above. The open symbols correspond to the thermal conductivity computed from the global 4234x5148 image resulting from the assembly of the 35 fields according to §2.

The first important result is that the average values of the 35 fields computed conductivities are very close to those obtained for the global field as it can be seen on figure 10.

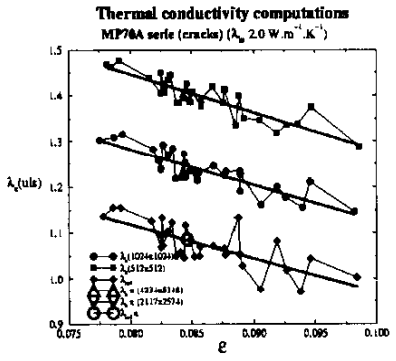

Figure 12: Crack contribution.

Therefore the decomposition in small (180x180 μm^2) domains with somewhat arbitrary boundary conditions leads to a correct estimation of the equivalent conductivity of a larger element of TBC.

The second important result comes from computations done for each class of porosity (Fig. 11 and 12).

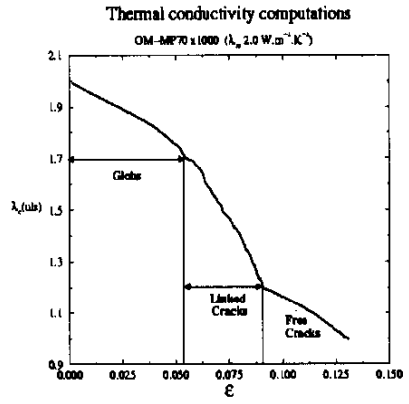

Figure 13: Influence of porosity class.

For almost identical porosity content, fields containing only the crack network present a thermal conductivity 10 to 30% smaller than that of fields with only globular pores. Analysis of computed conductivities reinforce the intuition that the major conductivity reduction results from the cracks which are mostly oriented in a direction perpendicular to the heat flow (see Fig. 4) in plasma sprayed TBCs.

This can be demonstrated even more clearly using porosity reconstruction (see §2) as computation input (Fig. 13). The rate of variation of the thermal conductivity with the porosity (e.g. $\partial\lambda_c/\partial\varepsilon$) strongly depends on the morphological class.

As the crack family has the highest rate of variation this class of porosity is the most efficient in reducing thermal conductivity in the case of plasma sprayed TBCs.

5. CONCLUSION

A software has been developed for the computation of the thermal conductivity of porous coatings (plasma sprayed TBCs) from binary images of real material cross sections. This approach based on a finite difference method takes directly into account the actual complex morphology of the ceramic which is mostly original with regard to existing models. This numerical model is able to determine the contribution of each morphological feature to the thermal conductivity and therefore compare different microstructures or coating architectures. In a near future it will be associated to a morphology generator for building a predictive tool. This one will be used in particular by engine manufacturers as guideline for modifying coating spraying conditions in order to obtain specific morphologies leading to optimised coating thermal properties.
It is important to note that this approach, developed on TBCs is most general and can be applied to a variety of multiphase media (refractories, composites, etc.).

Acknowledgements : Part of the work reported has been carried out within a Brite Euram project [4] and the support of the European Commission is gratefully acknowledged. Special thanks are due to SNECMA who provided the plasma sprayed coatings.

References

1. Sheffler K.D., Gupta D.K., « Current status and future trends in turbine application of thermal barrier coatings », J. Eng. Gas Turbines Power (Trans. ASME), 110, 1988, pp. 605-609.

2. Bose S. , DeMasi-Marcin J., « Thermal barrier coating experience in the gas turbine engine at Pratt & Whitney », in NASA CP 3312, 1995, pp. 63-78.

3. Thermal Barrier Coating Workshop. (Cincinnati, 19-21 may 1997)

4. High Insulation Thermal Barrier Systems. Brite Euram Project BE96-3226 (1996).

5. Youngblood G.E. , Rice R.W. , Ingel R.P., « Thermal diffusivity of partially and fully stabilised (yttria) zirconia single crystals », J. Am. Ceram. Soc. 71(4), 1988, pp. 255-260.

6. Hasselman D.P.H., Johnson L.F., Bentsen L.D., Syed R., Lee H.L.,Swain M.V., « Thermal diffusivity and conductivity of dense polycrystalline ZrO_2 ceramics : a survey », Am. Ceram. Soc. Bull. 66(5), 1987, pp. 799-806.

7. Kingery W.D., Bowen H.K., Uhlmann D.R., in « Introduction to ceramics ». J. Wiley (NY, 1976).

8. Madarasz F.L., Klemens P.G., « Reduction of lattice thermal conductivity by point defects at intermediate temperatures », Internat. J. Thermophysics. 8(2), 1987, pp. 257-262.

9. Maloney M.J., Achter H.S.,Barkalow B.K., « Development of low thermal conductivity thermal barrier coatings ». Communication presented in Thermal Barrier Coating Workshop (Cincinnati, may 1997).

10. Maxwell J.C., « Treatise on Electricity and Magnetism ». Oxford University Press.

11. Eucken A., « Thermal conductivity of ceramic refractory materials : calculation from thermal conductivity of constituents », VDI-Forschungsh. 353 (3-4), 1932, pp. 1-16.

12. Russel H.W., J. Am. Ceram. Soc. 18, 1939, p1.

13. Bruggeman D.A.G., « Berechnung Verschiedener Physikalischer Konstanten von Heterogenen Substanzen », Ann. Phys. 24(7), 1935, pp. 636-679.

14. Murabayashi M. et al., « Effect of porosity on the thermal conductivity of ThO_2 », J. Nucl. Sci. Tech. 6, 1969, p. 47

15.Schulz B., in High Temperature-High Pressure 13, 1981, pp 649-653.

16. Koh J.C., Fortini A., «Thermal conductivity and electrical resistivity of porous material », NASA report NAS3-12012, CR 1200854 (1971)

17. Cunningham M.E., Peddicord K.L., « Heat conduction in spheres packed in an infinite regular cubical array », Internat. J. Heat and Mass Transfer 24, 1991, pp1081-1088.

18. McLachlan D.S., Blaszkiewicz M., Newnham R.E., « Electrical resistance of composites », J. Am. Ceram. Soc. 73(8), 1990, pp 2187-21203.

19. Rhee S.K., « Porosity-thermal conductivity correlations for ceramic materials », Mat. Sci. Eng. 20, 1975, pp 89-93.

20. El-Fekey S.A., El-Mamoon Yehia M.,El-Hakim M.N., « Mathematical analysis of the dependence of thermal conductivity on porosity », Powder Met. Internat. 10(2), 1978, pp 90-91.

21. Jackson T.B., Virkar A.V., More K.L., Dinwiddie R.B., Cutler R.A., « High thermal conductivity aluminium nitride ceramics : the effect of thermodynamics, kinetic, and microstructural factors », J. Amer. Ceram. Soc. 80(6), 1997, pp 1421-1435.

22. Aizanov M.I., Domashnev I.A., in Poroshkovaya Met. 8,1968, p 51.

23.Bakker K., Kwast H., Cordfunke E.H.P., « The contribution of thermal radiation to the thermal conductivity of porous UO_2 », J. Nucl. materials 223, 1995, pp 135-142.

24. Da Yu Tzou, « A universal model for the overall thermal conductivity of porous media », J. Composite Materials 25, 1991, pp1064-1084.

25. Furmanski P., « Effective macroscopic description for heat conduction in heterogeneous materials », Int. J. Heat Mass Transfer 35(11), 1992, pp 3047-3058.

26. McPherson R., « A model for the thermal conductivity of plasma-sprayed ceramic coatings », Thin Solid Films 112, 1984, pp 89-95.

27. C. Moreau, S. Boire-Lavigne, R.G. Saint-Jacques, « The relationship between the microstructure and thermal diffusivity of plasma-sprayed tungsten coatings », in Proc. of the 7th National Thermal Spray Conference 20-24 June 1994, Boston (MA). Edited by C.C. Berndt and S. Sampath (ASM, 1994), pp 621-626.

28. Bjorneklett A., Haukeland L., Wigren J., Kristiansen H., « Effective medium theory and the thermal conductivity of plasma-sprayed ceramic coatings », J. Mat. Science 29, 1994, pp 4043-4050.

29. Hollis K.J., « Pore phase mapping and finite-element modelling of plasma sprayed tungsten coatings », in Advances in Thermal Spray Science and Technology. Proc. 8th National Thermal Spray Conference, 11-15 sept. 1995, Houston, Texas Edit. C.C. Berndt, S. Sampath (ASM), pp 403--408

30. Bakker K., « Using the finite element method to compute the influence of complex porosity and inclusion structures on the thermal and electrical conductivity », Int. J. heat Mass Transfer 40(15), 1997, pp 3503-3511.

31. Nogotov E.F., « Application of Numerical Heat Transfer », Series in Thermal and Fluids Engineering, McGraw-Hill Book Company,1978.

32. Peyret R., Taylor D., « Computational Methods for Fluid Flow », Springer-Verlag, 1986.

33. Orignac E., « Compared efficiencies of the conjugate gradient and the SOR methods applied to the solution of a three-dimensional laplacian », Private communication, ONERA 1997.

34. Anderson D.A., Tannehill J.C., Pletcher R.H.,
« Computational Fluid Mechanics and Heat Transfer », Hemisphere Publishing Corporation, 1984.